Hydrodynamic superradiance in wave-mediated cooperative tunneling

Konstantinos Papatryfonos, Mélanie Ruelle, Corentin Bourdiol, André Nachbin, John W M Bush, Matthieu Labousse

communications physics

ARTICLE

https://doi.org/10.1038/s42005-022-00918-y OPEN

Hydrodynamic superradiance in wave-mediated cooperative tunneling

Konstantinos Papatryfonos [1,2✉], Mélanie Ruelle[1], Corentin Bourdiol[1], André Nachbin [3✉], John W. M. Bush [2✉] & Matthieu Labousse [1]

Superradiance occurs in quantum optics when the emission rate of photons from multiple atoms is enhanced by inter-atom interactions. When the distance between two atoms is comparable to the emission wavelength, the atoms become entangled and their emission rate varies sinusoidally with their separation distance due to quantum interference. We here explore a theoretical model of pilot-wave hydrodynamics, wherein droplets self-propel on the surface of a vibrating bath. When a droplet is confined to a pair of hydrodynamic cavities between which it may transition unpredictably, in certain instances the system constitutes a two-level system with well-defined ground and excited states. When two such two-level systems are coupled through an intervening cavity, the probability of transition between states may be enhanced or diminished owing to the wave-mediated influence of its neighbour. Moreover, the tunneling probability varies sinusoidally with the coupling-cavity length. We thus establish a classical analog of quantum superradiance.

[1] Gulliver UMR CNRS 7083, ESPCI Paris, Université PSL, Paris 75005, France. [2] Department of Mathematics, MIT, 77 Massachusetts Ave., Cambridge, MA 02139, USA. [3] IMPA, Estrada Dona Castorina 110, Rio de Janeiro, RJ 22460-320, Brazil. ✉email: kpapatry@mit.edu; nachbin@impa.br; bush@math.mit.edu

In classical physics, particle motion is characterized in terms of dynamical states which may provide in turn the basis for a statistical description of the system. In quantum physics there is no such dynamical description: quantum systems are described entirely in terms of the evolution of their statistical states[1]. For a quantum system with at least two subsystems, non-separability arises when the quantum state cannot be factored into a product of states of its individual subsystems[2]. Many well-known bipartite quantum phenomena arise as a result of such non-separable states. One is the phenomenon of superradiance and subradiance, whereby the probability of decay of two coupled systems, as marked by photon emission, depends on the proximity of those systems[3–6].

Superradiance is a "cooperative" spontaneous emission of photons from a collection of N atoms that was theoretically predicted in 1954 by Robert Dicke[6]. When thermally excited atoms emit photons incoherently with respect to each other, the emitted intensity is proportional to the number of atoms, N. However, when the atoms radiate coherently, in phase with each other, the net electromagnetic field is proportional to N, and the emitted intensity thus scales as N^2. As a result, the atoms may decay at an enhanced rate that is up to N times faster than for incoherent emission, a phenomenon termed "superradiance".

When the distance between the atoms is of the order of the emission wavelength, rationalizing this collective behavior requires consideration of the system's quantum nature. The most elementary demonstration of Dicke's superradiance is achieved with two ions[4]. Experimentally, the photon emission rate $\Gamma(R)$ is characterized in terms of the inter-ion distance R, and compared to the single-ion emission rate Γ_0 in the same apparatus. The quantum theory describes a bipartite system in which two interacting two-level systems form a single four-level system. When far apart, the two subsystems are independent and can be either in the ground or excited states. When the two two-level systems interact, the collective system is treated as a single non-factorable four-level system, consisting of a ground state $|--\rangle$, degenerate first excited states $|+-\rangle$ or $|-+\rangle$ that are energetically indistinguishable, and a second excited (higher energy) state $|++\rangle$. Here $|+\rangle$ and $|-\rangle$ denote the states of the two subsystems, nomenclature that we adopt for our system. The decay rates $\Gamma_\pm$ to or from the degenerate excited states $|+-\rangle$ and $|-+\rangle$ are well-approximated by $\Gamma_\pm(R) = \Gamma_0\left(1 \pm \frac{3}{2}\frac{\sin(kR)}{kR} + \ldots\right)$ in the limit $kR \gtrapprox 10$, where $k = 2\pi/\lambda$ denotes the wavenumber and λ the emission wavelength[4]. Specifically, Γ_+ and Γ_- are the rates corresponding to transitions to or from the symmetric $(|+-\rangle + |-+\rangle)/\sqrt{2}$ and antisymmetric $(|+-\rangle - |-+\rangle)/\sqrt{2}$ states, respectively. We note that $\Gamma_\pm$ can be either greater or less than the bare emission rate Γ_0, corresponding to, respectively, superradiance or subradiance. The measured form of $\Gamma_\pm(R)$ was found to be in very good agreement with Dicke's theoretical prediction[4]. Such sinusoidally modulated, enhanced, or diminished radiance is an indirect measure of the nonseparability of states, a phenomenon commonly thought to be peculiar to the quantum realm.

Superradiance is a canonical effect in quantum optics with important applications in quantum communication[7]. Moreover, it was recently demonstrated that entangled free electrons may also exhibit superradiance through an emission pattern that cannot be accounted for by a classical mixed state[8], suggesting a means for non-destructive measurement[9] of entanglement between quantum systems. While a classical analog of superradiant emission has recently been reported in an experimental study of interfacial fracture[10], we here present an analog based on the hydrodynamic pilot-wave system[11,12].

Hydrodynamics has long served as a rich source of physical analogs for electromagnetic and optical phenomena[13–15]. More recently, it has yielded robust analogs of white holes[16], black holes[17,18], and rotational superradiant scattering[19]. Until recently, hydrodynamic analogs of quantum systems were relatively rare, but included the Aharanov–Bohm effect[20] and the Casimir effect[21]. The walking-droplet system discovered in 2005 by Yves Couder and Emmanuel Fort[11,22] has proven to be a remarkably rich source of physical analogs for both optical and quantum systems. This pilot-wave hydrodynamic system exhibits many features previously thought to be exclusive to the quantum realm, and so has initiated the burgeoning field of hydrodynamic quantum analogs[12,23,24].

Couder and Fort[11] discovered a classical pilot-wave system that consists of a millimetric droplet bouncing on the surface of a vibrating liquid bath, self-propelling by virtue of a resonant interaction with its own wave field. By virtue of this resonance, the droplet is accompanied by a quasi-monochromatic wave field that imposes a dynamic constraint on the droplet that gives rise to the emergence of quantized dynamical states[12]. For example, quantized orbital states emerge when the walking droplets move in the presence of either Coriolis[25–27] or central spring forces[28–30] and Bohr–Sommerfeld quantization may emerge for walkers in a harmonic well[31]. Features of quantum optics have also been captured, including single-particle diffraction and interference[22,32,33] and the Hong-Ou-Mandel effect[34]. The persistence of the pilot-wave field renders the drop dynamics non-Markovian[35,36]; specifically, the instantaneous wave force imparted to the drop during impact depends on the particle's history. The droplet thus navigates a potential landscape of its own making. The non-Markovian feature of the droplet dynamics gives rise to behavior that might be mistakenly inferred to be spatially non-local if the influence of the wave field is not adequately resolved[24]. Of particular interest, here is the hydrodynamic analog of unpredictable quantum tunneling[37], as has been demonstrated both experimentally[38,39] and numerically[40,41].

We introduce here a theoretical model of bipartite tunneling in the hydrodynamic pilot-wave system that allows us to establish a classical analog of quantum superradiance. We do so by satisfying three criteria. First, we consider a classical two-level system in which one of the two states may be treated as the lower-energy state, in the sense that it is more likely to arise. Second, we produce a bipartite system, consisting of two such two-level systems, coupled in such a way that their collective behavior cannot be specified in terms of a linear combination of its individual subsystems. Third, we demonstrate that the probability of transition from state to state in each subsystem varies in a sinusoidal fashion with the distance between the two subsystems.

Results

Model dynamics. Our model system comprises two subsystems, labeled 1 and 2 in Fig. 1a, each consisting of a wave-generating particle in an identical pair of cavities separated by a barrier across which the particle may tunnel. Each particle generates waves and moves in response to them in a manner detailed in "Methods". The two subsystems are separated by a coupling cavity of variable width L_c, and by barriers that are sufficiently high as to preclude the particles from tunneling into the coupling cavity. The particles are thus confined to one of the two subsystems, but may find themselves in either the inner or outer cavities of their subsystem. Each of the four cavities has a fixed length of $L = 1.2$ cm, corresponding to $\sim 2.5\lambda_F$. Here, λ_F is the Faraday wavelength, the most unstable wavelength of the vibrating bath, and the dominant wavelength of the droplet's pilot-wave field[11,22].

Each bouncing droplet, within its two-level system, generates waves that are reflected and transmitted as they interact with the bottom topography. The coupling cavity is relatively deep and so closer to the Faraday threshold; thus, waves transmitted into it are relatively persistent and so capable of influencing the other two-

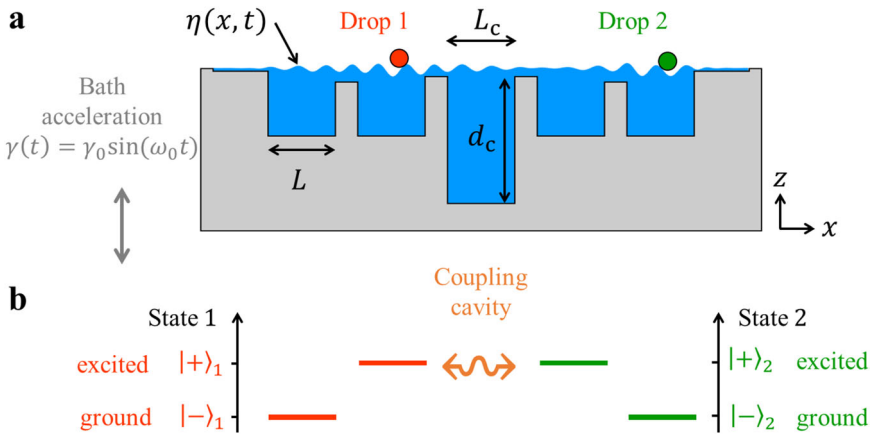

Fig. 1 Description of the numerical model of two coupled, two-levels systems. a The model system consists of a pair of drops (red and green) walking on the surface of a vibrating fluid bath (blue) that spans the solid substrate (gray). Each drop is confined to a pair of wells separated by barriers across which they may tunnel unpredictably. The extent of coupling in this bipartite tunneling system is prescribed by the magnitude of the vertical vibrational forcing, γ_0, angular frequency, ω_0, and the width, L_c, of the intervening coupling cavity, a region that is forbidden to both drops. **b** The state of each droplet is denoted by $|-\rangle$ or $|+\rangle$ according to whether the drops are in, respectively, the outer "ground" state or the inner "excited" state.

level system. The central cavity thus establishes the long-range coupling between the two two-level systems. The efficiency of this coupling is prescribed by the geometry of the central cavity: by increasing its depth d_c, the coupling is increased, allowing the coupling cavity to serve as a nearly resonant transmission line[42].

In all simulations, we set the coupling cavity depth to $d_c = 6.3\lambda_F$ which ensures strong intercavity coupling. In subsystems 1 and 2, the particle may tunnel between the outer and inner cavities, but the probability of presence in these cavities is not generally 50%. Specifically, in the geometry considered, the particles are more likely to be in the outer cavity. We thus describe our bipartite tunneling system in terms of two coupled, two-level systems, as shown in Fig. 1b.

Tunneling. When a single droplet is placed in one of the two subsystems, the single-particle tunneling probability (Γ_0) may be deduced by counting the number of tunneling events per crossing attempt over a sufficiently long time interval. When the two droplets are placed in each of the two subsystems, the tunneling probabilities change substantially from Γ_0, owing to the wave-mediated coupling of the two subsystems. Figure 2a, b indicates that the probability of tunneling increases substantially when the second droplet is present in the neighboring system, an effect akin to superradiance. Figure 2c, d presents a configuration with a longer coupling cavity in which the tunneling probability is substantially decreased by the addition of a neighbor, corresponding to subradiance.

Having established that wave-mediated coupling alters the tunneling probability in this bipartite system, we proceed by characterizing the dependence of the transition probabilities on the system geometry. Figure 3a illustrates how the tunneling probability depends on the length of the coupling cavity, L_c. The tunneling probability either increases or decreases relative to Γ_0, varying continuously with L_c in an oscillatory fashion, reminiscent of the modulation of the emission rate reported in ion-pair quantum mechanical superradiance[4]. Further to this modulation, the peaks become less intense and slightly broader as L_c increases, a trend that is likewise apparent in quantum superradiance[4]. For $L_c/\lambda_F > 6$, the single-drop and droplet-pair crossing probabilities largely coincide, indicating that the two components of this bipartite system behave as if they were uncoupled. Specifically, the tunneling probability of a particular drop is determined by the length of the coupling cavity, but unaffected by its distant neighbor.

Rationalizing transition probabilities. The evolution of the transition probability with coupling-cavity length is rationalized in Fig. 3b, where we report the difference in oscillator action $\delta A_{\text{total}}(L_c) = A^+(L_c) - A^-$ (as defined in Eq. (4) of "Methods") between the excited and ground states. For the one-drop system, the oscillator action difference is a constant which is independent on L_c (see Supplementary Fig. 1 for the details of all the contributions). For the two-drops system, the oscillator action in the inner cavity is constant (see Supplementary Fig. 2), independent of L_c, and we take its mean value A^- as a reference. Conversely, the oscillator action in the outer cavity varies significantly with coupling-cavity length L_c; we denote its value by $A^+(L_c)$. A comparison between Fig. 3a and b shows a direct correspondence between the maxima and minima of the transition probability and the minima and maxima of δA_{total}, respectively. We conclude that the wave-mediated lowering of the oscillator action strongly favors the transition from the ground to the excited states. The one-droplet system simulations reveal a difference of oscillator action δA_{total} that is approximately constant for sufficiently small coupling-cavity length $L_c < 6\lambda_F$.

We further note that when $L_c/\lambda_F < 1$ the mid-cavity is a relatively deep, slender region, which poses problems for the nonlinear solver of the numerical conformal mapping. This limitation is presumably due to the crowding phenomenon, a numerical conformal mapping feature arising when two pre-images of vertices get exponentially close in the canonical domain[43]. The gray region in Fig. 3 identifies these slender coupling cavities that could not be reliably explored numerically.

Finally, we examine the correlation between the wavefield structure and the particle dynamics. Figure 4a illustrates both the particle positions and instantaneous wave field. An assessment of the wave intensity (Eq. (5) in "Methods") in each cavity is shown in Fig. 4b–d. Each cavity is color-coded for ease of reference. The rightmost panel shows the wave intensity of the system across all cavities. Periods in which one particle has tunneled into an excited state are denoted by light gray. Such intervals are accompanied by a reversal in the relative wave intensity in the inner and outer cavities, and an increase in the wave intensity in the coupling cavity. Periods in which both particles are in excited states are denoted by dark gray, and marked by maxima in the wave intensity in the coupling cavity and minima in the global wave intensity. The wave intensity diagnostic thus provides rationale for associating the outer and inner cavities with, respectively, ground and excited states.

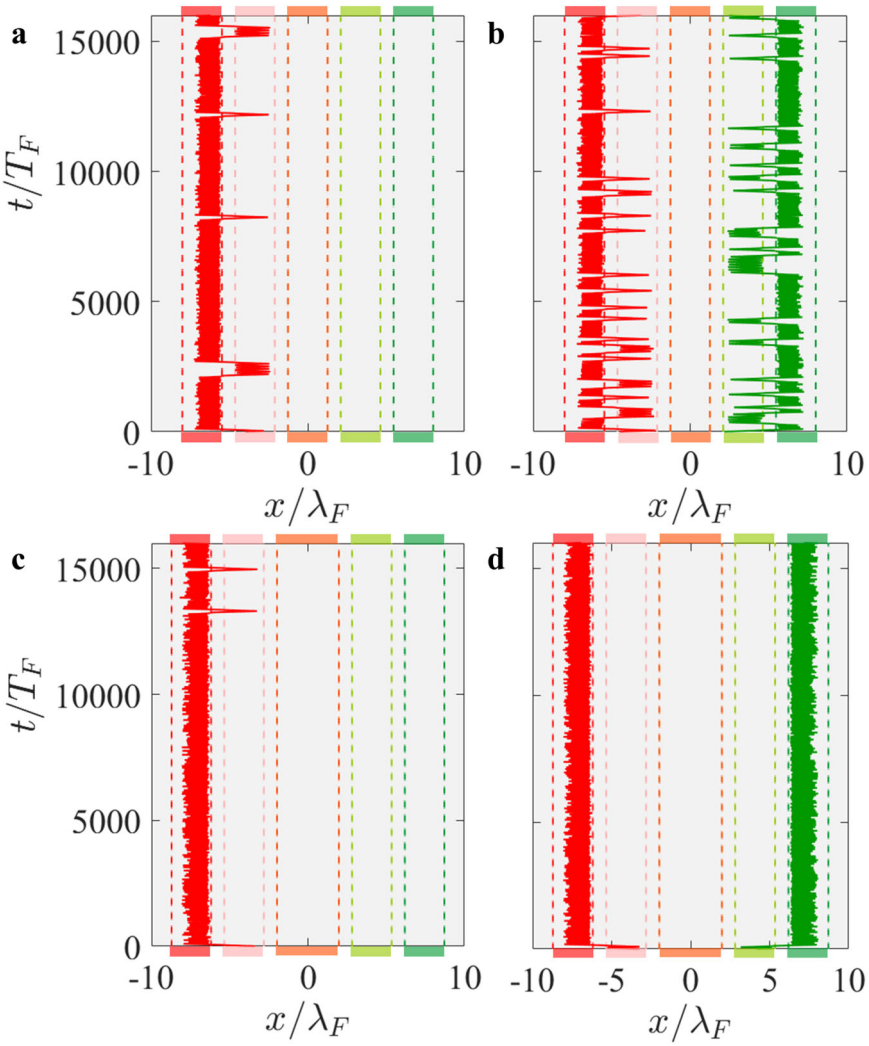

Fig. 2 Tunneling dynamics and trajectories of the drops. a A single droplet tunnels between its ground state (outer cavity) and excited state (inner cavity). The middle cavity (marked in orange) couples the left and right subsystems. The red and green lines denote the particle paths in the left and right subsystems, respectively. Dashed lines indicate the edges of the various cavities. **b** In the bipartite system, a pair of drops tunnel between their ground and excited states. In (**a**, **b**), the coupling-cavity length is $L_c = 2.44\lambda_F$ and the four other cavities' lengths are $L = 2.52\lambda_F$. Comparing (**a**) and (**b**), makes clear that a single particle's tunneling probability is substantially increased by the presence of a neighboring drop, corresponding to superradiance. The configuration shown in (**c**, **d**) is similar to (**a**) and (**b**) but with a larger coupling cavity $L_c = 3.96\lambda_F$. Comparing (**c**) and (**d**) reveals that the particle's tunneling between cavities is inhibited by the presence of the neighboring drop, an effect corresponding to subradiance.

Discussion

We have examined a model of bipartite tunneling in a classical system. The tunneling probability within the two subsystems is mediated by their common wave field and shown to depend on the length of the coupling cavity. This dependence is similar to that of the probability of photon emission on inter-ion spacing in the case of quantum superradiance (e.g., compare our Fig. 2 with Figs. 2 and 6 of ref. [4]). If we consider that the energy stored in our system is altered each time the droplet tunnels between the ground and excited states, we can establish a direct analogy between our system and quantum superradiance. Specifically, we may identify the alteration of the wave field that accompanies the transition from a high-energy to lower-energy state with the emission of a photon in quantum mechanics. Thus, the probability of tunneling is directly analogous to the transition rate in superradiant photon emission.

We have highlighted the similarities between our classical system of bipartite tunneling and super- or subradiant photon emission from ion pairs. To account for the optical superradiance in quantum mechanics, one must invoke the concept of collective, non-separable, states that are formed between the two ions, which are viewed as absorbing or emitting each photon collectively[4,7,44,45]. Quantum mechanics offers no physical picture for the origins of non-separable states, only the mathematical tools required to calculate the relevant probability densities. Our system illustrates how such correlations may arise in a classical, wave-mediated system. The correlations in our system arise from the wave coupling between the two tunneling subsystems. While the form of the waves may be deduced by linear superposition, their influence on the tunneling probability is nonlinear. Specifically, the discrete tunneling events are unpredictable, as they depend in a subtle fashion on the interactions between the particles, the waves and the underlying potential wells formed by bottom topography[39,40,46].

A hydrodynamic analog of superradiant emission was recently realized experimentally in a distinct fluidic system. Specifically, drops were produced via vibration-induced interfacial fracture from adjacent circular cavities coupled through a thin layer, and the rate of droplet ejection was seen to vary sinusoidally with the distance between the cavities[10]. Table 1 summarizes the key physical analogies between superradiant emission as arises in

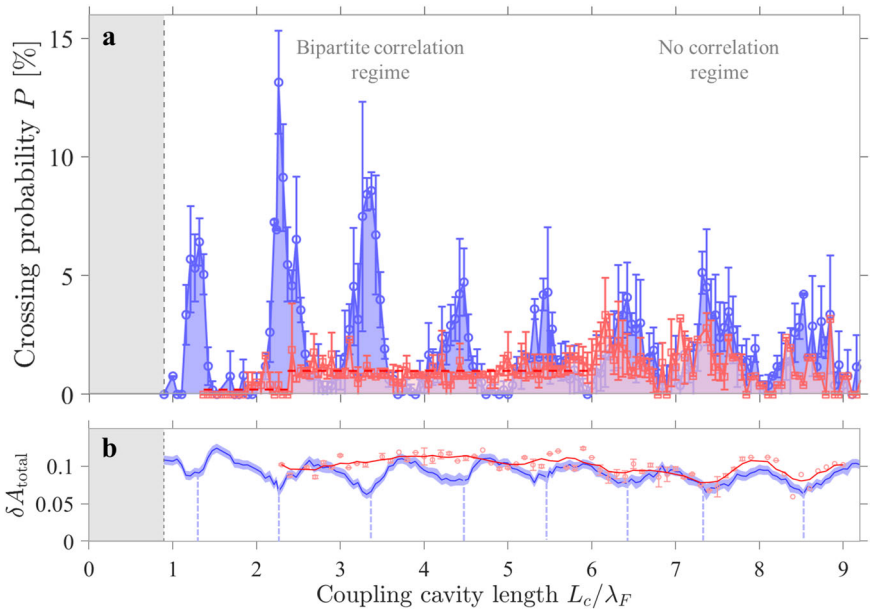

Fig. 3 Evolution of the transition probability with the width of the coupling cavity. a The dependence of the probability of tunneling from the outer to the inner cavity on the width of the coupling cavity, L_c, for a single drop (red squares) and for two drops (blue circles). The red dashed line is the average tunneling probability for a single drop for coupling cavity lengths $L_c/\lambda_F < 6$. For $2.3 < L_c/\lambda_F < 6$ this average probability $\langle P \rangle = 1.0\%$ (95% confidence interval [0.91:1.09]). Error bars represent the standard deviation over six independent numerical runs. **b** Evolution of the energy barrier to tunneling, δA_{total}, for the two-droplet system (blue) and the one-droplet system (red). Blue shaded regions adjoining the lines denote the error bars. Note that the probability maxima in panel **a** correspond to energy-barrier minima in **b**. For $L_c/\lambda_F > 6$, the tunneling probability of either drop converges to that of a single droplet, and so is evidently unaffected by its distant neighbor. The gray region on the left denotes the region of tall, slender coupling cavities that could not be reliably explored numerically.

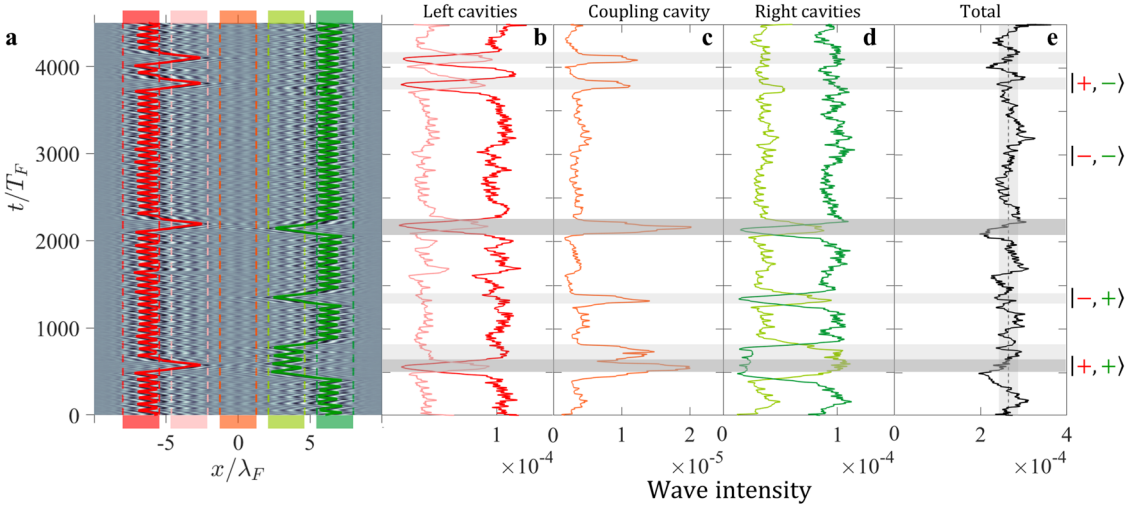

Fig. 4 Wave intensity. a The particle paths and associated wave fields. Light and dark regions correspond to wave minima and maxima, respectively. **b**–**e** The associated wave intensity, as computed from Supplementary Eq. (3). Comparison of (**a**) and (**b**) reveals the correlation between extrema in the wave intensity and the tunneling events. In (**b**–**e**), intervals in which one or both drops are in an excited state are denoted by light and dark gray, respectively, and are correlated with local extrema in the total wave intensity.

quantum optics, droplet emission via interfacial fracture[10], and the bipartite droplet tunneling considered here.

Experimental realization of the one-dimensional dynamics considered here would require that one confine the walking droplets to a narrow channel, of width comparable to the Faraday wavelength. Indeed, we have already used such confinement to study the synchronization of drop-pairs in a three-cavity geometry[47] and extension to the five-cavity geometry considered here should be possible. While one does not expect quantitative agreement between our numerical model and such an experimental realization owing to the heightened dissipation associated with the three-dimensional laboratory flows, one does expect to be able to capture qualitative features such as the superradiant tunneling reported here.

In the study of hydrodynamic quantum analogs, we are generally satisfied with qualitative analogs, the demonstration of which is sufficient to challenge the prevailing notion that quantum systems are entirely inscrutable from a classical perspective[24]. While there are hydrodynamic analogs that exhibit behavior quantitatively similar to their quantum counterparts, including Friedel oscillations[48] and quantum corrals[49,50], more commonly the analogy is at the qualitative level, as in the case of

Table 1 Comparison of quantum superradiant photon emission from ion pairs[4], the hydrodynamic analog of ref. [10] and that developed here.

	Quantum optics[4]	Interfacial fracture[10]	Hydrodynamic tunneling
Emission event	Photon emission	Droplet emission	Droplet tunneling
Characteristic wavelength	Emission wavelength	Faraday wavelength	Faraday wavelength
Origins of superradiance	Quantum (wave function) interference	Faraday wave interference	Faraday wave interference

the bipartite tunneling system studied here. Nevertheless, we believe that the study of hydrodynamic quantum analogs complements more traditional studies of quantum systems in providing a perspective and platform for assessing which quantum effects can and cannot be understood from a classical perspective.

Our bipartite tunneling system has given rise to collective transition statistics, specifically subradiant and superradiant tunneling rates between the ground and excited states, which may be predictably controlled by altering the distance between the two two-level systems. Notably, the precise energetic difference between the ground and excited states may be altered and even reversed by changing the geometry of the outer cavities (Supplementary Fig. 3 and Supplementary Note 3). Our system thus provides a platform for characterizing wave-induced correlations between particle pairs. Specifically, by taking the system geometry as a proxy for measurement settings, we intend to test the viability of violating Bell-type inequalities with this classical pilot-wave system[51].

Methods

Numerical method. Nachbin et al.[40] formulated a theoretical model for the one-dimensional motion of a walking droplet over a vibrating liquid bath with complex topography. Here, we adapt this model in order to consider two identical particles in the multiple-cavity geometry depicted schematically in Fig. 1. The positions, X_j ($j = 1, 2$), of the two identical particles of mass m evolve according to Newton's Law:

$$m\ddot{X}_j + c\,F(t)\dot{X}_j = -F(t)\,\frac{\partial \eta}{\partial x}(X_j(t), t). \tag{1}$$

The particle moves in response to gradients of the wave elevation $\eta(x, t)$, which thus plays the role of a time-dependent potential. The particle motion is resisted by a drag force proportional to its speed. The drag constant c follows from the modeling presented in refs. [52,53]. The time dependence of the propulsive and drag forces reflects that of the reaction force, $F(t)$, acting on the drop during its contact with the bath[52,53]. In terms of their lateral motion, the particles are viewed as oscillators that can transition unpredictably between two neighboring cavities.

The particles serve as moving wave sources that establish their own time-dependent wave potential that is computed as follows. The velocity potential of the liquid bath $\phi(x, z, t)$ is a harmonic function satisfying Laplace's equation. In the bulk of the fluid, the velocity field is given by $(u, v) = \nabla\,\phi$. The fluid bath has density 0.95 g/cm^3, viscosity 16cS and surface tension 20.9 dynes/cm, values typical of silicone oil, and oscillates vertically with frequency $\omega_0/2\pi = 80$ Hz. The resonant bouncing of the particle at the Faraday frequency triggers a monochromatic damped wave pattern with a corresponding deep-water Faraday wavelength of $\lambda_F = 4.75$ mm. The wave model is formulated in the bath's reference frame, where the effective gravity is $g(t) = g(1 + \gamma_0 \sin(\omega_0 t))$, where g is the acceleration due to gravity, $\gamma_0 = A_0\omega_0^2/g$ the maximum dimensionless vibrational acceleration, and A_0 the amplitude of vibration. We here fix $\gamma_0 = 4.21$ (90.3% of the Faraday threshold, $\gamma_F = 4.66$), where superradiant effects are pronounced, as indicated by an initial parameter sweep. The wave field thus evolves according to refs. [40,53]:

$$\frac{\partial \eta}{\partial t} = \frac{\partial \phi}{\partial z} + 2\nu\frac{\partial^2 \eta}{\partial x^2}, \tag{2}$$

$$\frac{\partial \phi}{\partial t} = -g(t)\eta + \frac{\sigma}{\rho}\frac{\partial^2 \eta}{\partial x^2} + 2\nu\frac{\partial^2 \phi}{\partial x^2} - \sum_{j=1,2}\frac{P_d(x - X_j(t))}{\rho}. \tag{3}$$

The particles ($j = 1, 2$) generate waves on the free surface by applying local pressure terms P_d. The wave forcing term $P_d(x - X_j(t))$ and the coefficient $F(t)$ are activated only during a fraction of the Faraday period T_F, corresponding to the contact time T_c in the walking-droplet system and approximated by $T_c = T_F/4$. The particle is assumed to be in resonance with the most unstable (subharmonic) Faraday mode of the bath[53], a key feature of pilot-wave hydrodynamics[12,24,54]. Further details and discussion concerning the numerical implementation of the model system, (1) and (2)–(3) are provided in the Supplementary Note 1.

System's energetics. We proceed by defining the diagnostics that characterize the system's energetics. For nearly periodic cycles, we characterize the particle energy in phase space. We define a cycle-averaged energy quantity for particle $j = 1, 2$

$$\bar{A}_j = \int_t^{t+T}\left[\bar{\Omega}_0 X_j^2(t) + \bar{\Omega}_0^{-1}\dot{X}_j^2(t)\right]dt \tag{4}$$

that we refer to as the "oscillator action", a name originating from conserved quantities used to describe wave propagation in fluids[55]. $\bar{A}_j$ is calculated over the period T of a given cycle; the associated mean angular frequency $\bar{\Omega}_0$ is readily computed numerically. We note that $\bar{A}^{1/2}$ is a length related to the range of droplet excursions within a cavity. Notably, $\bar{A}$ is lower in the ground state than in the excited state in all geometries considered here: excited states are marked by relatively large particle excursions. We denote by δA_{total} the energetic barrier to tunneling between two states.

As a diagnostic for the wave energy, we monitor the wave intensity:

$$||\eta||(t) = \left(\int \left(\eta(x, t)\right)^2 dx\right)^{1/2}. \tag{5}$$

Further details and discussion concerning the diagnostics (4) and (5) are provided in the Supplementary Note 2.

Data availability

The data that support the findings of our study are available upon request.

Code availability

The code that generated the data is available upon request.

Received: 4 January 2022; Accepted: 16 May 2022;
Published online: 08 June 2022

References

1. Cohen-Tannoudji, C., Diu, B. & Laloë, F. *Quantum Mechanics*, 1st edn. (Wiley, 1977).
2. Popescu, S. & Rohrlich, D. Generic quantum nonlocality. *Phys. Lett. A* **166**, 293–297 (1992).
3. Solano, P., Barberis-Blostein, P., Fatemi, F. K., Orozco, L. A. & Rolston, S. L. Super-radiance reveals infinite-range dipole interactions through a nanofiber. *Nat. Commun.* **8**, 1857 (2017).
4. DeVoe, R. G. & Brewer, R. Observation of superradiant and subradiant spontaneous emission of two trapped ions. *Phys. Rev. Lett.* **76**, 2049–2052 (1996).
5. Eschner, J., Raab, C., Schmidt-Kaler, F. & Blatt, R. Light interference from single atoms and their mirror images. *Nature* **413**, 495–498 (2001).
6. Dicke, R. H. Coherence in spontaneous radiation processes. *Phys. Rev.* **93**, 99–110 (1954).
7. Scully, M. O. & Svidzinsky, A. A. The super of superradiance. *Science* **325**, 1510–1511 (2009).
8. Karnieli, A., Rivera, N., Arie, A. & Kaminer, I. Superradiance and subradiance due to quantum interference of entangled free electrons. *Phys. Rev. Lett.* **127**, 060403 (2021).
9. Reiserer, S., Ritter, S. & Rempe, G. Nondestructive detection of an optical photon. *Science* **342**, 1349–1351 (2013).
10. Frumkin, V., Papatryfonos, K. & Bush, J. W. M. A hydrodynamic analog of superradiant emission. Preprint at https://arxiv.org/pdf/2111.04687.pdf (2021).
11. Couder, Y., Protière, S., Fort, E. & Boudaoud, A. Walking and orbiting droplets. *Nature* **437**, 208 (2005).
12. Bush, J. W. M. Pilot-wave hydrodynamics. *Ann. Rev. Fluid Mech.* **47**, 269–292 (2015).
13. Young, T. The Bakerian lecture: experiments and calculations relative to physical optics. *Phil. Trans. Roy. Soc. Lond.* **94**, 1–16 (1804).

14. Bragg, W. L. & Nye, J. F. A dynamical model of a crystal structure. *Proc. R. Soc. Lond. A* **190**, 474–481 (1947).
15. Bush, J. W. M. The new wave of pilot-wave theory. *Phys. Today* **68**, 47–53 (2015).
16. Jannes, G., Piquet, R., Maïssa, P., Mathis, C. & Rousseaux, G. Experimental demonstration of the supersonic-subsonic bifurcation in the circular jump: a hydrodynamic white hole. *Phys. Rev. E* **83**, 056312 (2011).
17. Schützhold, R. & Unruh, W. Gravity wave analogues of black holes. *Phys. Rev. D* **66**, 044019 (2002).
18. Nardin, J.-C., Rousseaux, G. & Coullet, P. Wave-current interaction as a spatial dynamical system: analogies with rainbow and black hole physics. *Phys. Rev. Lett.* **102**, 124504 (2009).
19. Torres, T. et al. Rotational superradiant scattering in a vortex flow. *Nat. Phys.* **13**, 833–836 (2017).
20. Berry, M. V., Chambers, R. G., Large, M. D., Upstill, C. & Walmsley, J. C. Wavefront dislocations in the Aharanov-Bohm effect and its water wave analogue. *Eur. J. Phys.* **1**, 154–162 (1980).
21. Denardo, B. C., Puda, J. J. & Larraza, A. A water wave analog of the Casimir effect. *Am. J. Phys.* **77**, 1095–1101 (2009).
22. Couder, Y. & Fort, E. Single particle diffraction and interference at a macroscopic scale. *Phys. Rev. Lett.* **97**, 154101 (2006).
23. Bush, J. W. M., Couder, Y., Gilet, T., Milewski, P. A. & Nachbin, A. Introduction to focus issue on hydrodynamic quantum analogues. *Chaos* **28**, 096001 (2018).
24. Bush, J. W. M. & Oza, A. U. Hydrodynamic quantum analogs. *Rep. Progress Phys.* **84**, 017001 (2020).
25. Fort, E., Eddi, A., Moukhtar, J., Boudaoud, A. & Couder, Y. Path-memory induced quantization of classical orbits. *Proc. Natl. Acad. Sci. USA* **107**, 17515–17520 (2010).
26. Harris, D. M. & Bush, J. W. M. Drops walking in a rotating frame: from quantized orbits to multimodal statistics. *J. Fluid Mech.* **739**, 444–464 (2014).
27. Oza, A. U., Wind-Willassen, O., Harris, D. M., Rosales, R. R. & Bush, J. W. M. Pilot-wave hydrodynamics in a rotating frame: exotic orbits. *Phys. Fluids* **26**, 082101 (2014).
28. Perrard, S., Labousse, M., Miskin, M., Fort, E. & Couder, Y. Self-organization into quantized eigenstates of a classical wave-driven particle. *Nat. Commun.* **5**, 1–8 (2014).
29. Labousse, M. & Perrard, S. Non-Hamiltonian features of a classical pilot-wave dynamics. *Phys. Rev. E* **90**, 022913 (2014).
30. Labousse, M., Perrard, S., Couder, Y. & Fort, E. Self-attraction into spinning eigenstates of a mobile wave source by its emission back-reaction. *Phys. Rev. E* **94**, 042224 (2016).
31. Montes, J., Revuelta, F. & Borondo, F. Bohr-Sommerfeld-like quantization in the theory of walking droplets. *Phys. Rev. E* **103**, 053110 (2021).
32. Pucci, G., Harris, D. M., Faria, L. M. & Bush, J. W. M. Walking droplets interacting with single and double slits. *J. Fluid Mech.* **835**, 1136–1156 (2018).
33. Ellegaard, C. & Levinsen, M. T. Interaction of wave-driven particles with slit structures. *Phys. Rev. E* **102**, 023115 (2020).
34. Valani, R. N., Slim, A. C. & Simula, T. Hong-ou-Mandel-like two-droplet correlations. *Chaos* **28**, 096104 (2018).
35. Perrard, S. & Labousse, M. Transition to chaos in wave memory dynamics in a harmonic well: Deterministic and noise-driven behavior. *Chaos* **28**, 096109 (2018).
36. Budanur, N. B. & Fleury, M. State space geometry of the chaotic pilot-wave hydrodynamics. *Chaos* **29**, 013122 (2019).
37. Papatryfonos, K. et al. One-dimensional nature of inas/inp quantum dashes revealed by scanning tunneling spectroscopy. *Nano Letters* **15**, 4488–4497 (2015).
38. Eddi, A., Fort, E., Moisy, F. & Couder, Y. Unpredictable tunneling of a classical wave-particle association. *Phys. Rev. Lett.* **102**, 240401 (2009).
39. Tadrist, L., Gilet, T., Schlagheck, P. & Bush, J. W. M. On predictability in a hydrodynamic pilot-wave system: resolution of walker tunneling. *Phys. Rev. E* **102**, 013104 (2020).
40. Nachbin, A., Milewski, P. A. & Bush, J. W. M. Tunneling with a hydrodynamic pilot-wave model. *Phys. Rev. Fluids* **2**, 034801 (2017).
41. Hubert, M., Labousse, M. & Perrard, S. Self-propulsion and crossing statistics under random initial conditions. *Phys. Rev. E* **95**, 062607 (2017).
42. Nachbin, A. Walking droplets correlated at a distance. *Chaos*, **28**, 096110 (2018).
43. Driscoll, T. & Trefethen, L. *Schwarz-Christoffel Mapping* (Cambridge University Press, 2002).
44. Makarov, A. A. & Letokhov, V. S. Spontaneous decay in a system of two spatially separated atoms (One-dimensional case). *J. Exp. Theor. Phys.* **97**, 688–701 (2003).
45. Makarov, A. A. & Letokhov, V. S. Metastable entangled states of atomic systems in macroscale: radiation dynamics and spectrum. In *International Workshop on Quantum Optics 2003 (Proceedings of the SPIE)* 54–64 (SPIE, 2004).
46. Eddi, A., Terwagne, D., Fort, E. & Couder, Y. Wave propelled ratchets and drifting rafts. *Europhys. Lett.* **82**, 44001 (2008).
47. Nachbin, A., Couchman, M. M. P. & Bush, J. W. M. Non-local features of a hydrodynamic pilot-wave system. http://meetings.aps.org/Meeting/DFD16/Session/L16.5 (2016).
48. Sáenz, P. J., Cristea-Platon, T. & Bush, J. W. M. A hydrodynamic analog of Friedel oscillations. *Sci. Adv.* **6**, eaay9234 (2020).
49. Harris, D. M., Moukhtar, J., Fort, E., Couder, Y. & Bush, J. W. M. Wavelike statistics from pilot-wave dynamics in a circular corral. *Phys. Rev. E* **88**, 1–5 (2013).
50. Sáenz, P. J., Cristea-Platon, T. & Bush, J. W. M. Statistical projection effects in a hydrodynamic pilot-wave system. *Nat. Phys.* **14**, 315–319 (2018).
51. Vervoort, L. Are hidden-variable theories for pilot-wave systems possible? *Found. Phys.* **48**, 803–826 (2018).
52. Moláček, J. & Bush, J. W. M. Drops walking on a vibrating bath: towards a hydrodynamic pilot-wave theory. *J. Fluid Mech.* **727**, 612–647 (2013).
53. Milewski, P., Galeano-Rios, C., Nachbin, A. & Bush, J. W. M. Faraday pilot-wave dynamics: modelling and computation. *J. Fluid Mech.* **778**, 361–388 (2015).
54. Protière, S., Boudaoud, A. & Couder, Y. Particle-wave association on a fluid interface. *J. Fluid. Mech.* **554**, 85–108 (2006).
55. Andrews, D. & McIntyre, M. On wave action and its relative. *J. Fluid Mech.* **89**, 647 (1978).

Acknowledgements

The authors acknowledge the financial support of the NSF through grants CMMI-1727565 and CMMI-2154151, the European Union's Horizon 2020 Research and Innovation Program under the Marie Sklodowska-Curie project EnHydro, grant No. 841417, and the CNPq under (PQ-1B) 301949/2007-7, and FAPERJ Cientistas do Nosso Estado Project No. 150.036/2018.

Author contributions

J.B., M.L., K.P., and A.N. designed and coordinated the studies. A.N. create the numerical model. K.P., M.R., and C.B. performed the numerical simulations. K.P., M.R., C.B., and M.L. analyzed the results. A.N., J.B., M.L., and K.P. contributed to the writing of the paper. All authors have read and agreed to the published version of the manuscript.

Competing interests

The authors declare no competing interests.

Additional information

Supplementary information The online version contains supplementary material available at https://doi.org/10.1038/s42005-022-00918-y.

Correspondence and requests for materials should be addressed to Konstantinos Papatryfonos, André. Nachbin or John W. M. Bush.

Peer review information *Communications Physics* thanks Germain Rousseaux, Florentino Borondo, Rahil Valani and Nazmi Burak Budanur for their contribution to the peer review of this work. Peer reviewer reports are available.